

Article

A DFT Insight into the Tuning Effect of Potassium Promoter on the Formation of Carbon Atoms via Carburization Gases Dissociation on Iron-Based Catalysts

Juhui Gong, Cheng Cao, Ruiqin Sun, Linxia Cui, Rui Gao and Haigang Hao *

College of Chemistry and Chemical Engineering, Inner Mongolia University, Hohhot 010021, China; imugongjuhui@163.com (J.G.); imuhgcch@163.com (C.C.); imusunruiqin@163.com (R.S.); imucuilinxia@163.com (L.C.); gaorui@imu.edu.cn (R.G.)

* Correspondence: haohaigang@imu.edu.cn

Received: 21 April 2020; Accepted: 7 May 2020; Published: 10 May 2020



Abstract: The research of the formation mechanism of iron carbides is significant to design the high-performance catalysts for the Fischer–Tropsch synthesis (FTS) process. In this paper, the effect of potassium promoter on the formation of atomic carbon via carburization gases dissociation on the iron-based catalyst, the C_2H_4 , C_2H_2 and CO/H_2 adsorption energies and dissociation paths as well as the rate constants of the corresponding elementary steps are investigated by DFT on the Fe(110), Fe(110)- K_2O , Fe(211) and Fe(211)- K_2O surfaces. The calculation results demonstrated that the K_2O promoter can modify the capabilities of surface C formation via the thermodynamic method as well as the kinetical method. The K_2O promoter can increase the CO adsorption energy while decreasing the C_2H_4 adsorption energy both on Fe(110) and Fe(211) surfaces. Kinetically, via tuning the catalyst surfaces from Fe(110) to Fe(211), the K_2O promoter can inhibit the ability of C_2H_4/C_2H_2 dissociation to atomic carbon, while enhancing the ability of CO/H_2 decomposition to atomic carbon. The C_2H_4/C_2H_2 dissociation rate constants on Fe(211) and Fe(211)- K_2O are about 10^7 times slower than that on Fe(110) and Fe(110)- K_2O , whereas the dissociation rate constants of CO/H_2 on Fe(211) are about 10^6 times faster than that on Fe(110), and about 10^7 times faster on Fe(211)- K_2O than on Fe(110)- K_2O .

Keywords: DFT; Fischer-Tropsch synthesis; dissociation; potassium; iron-based catalyst

1. Introduction

Owing to the lack of crude oil, Fischer–Tropsch synthesis (FTS), which converts syngas (CO and H_2) into valuable chemicals and clean fuels, is of important academic and commercial significance in China. The catalyst is one of the most key factors account for the successes of the industrial FTS process, and the iron-based catalysts are extensively studied and used for decades due to their low cost and relative high activity [1–5]. It is well known that the main active phases are iron carbides in the iron-based FTS [6–8]. However, because of the complex phase transformations, numerous iron carbide phases can be formed during the carburization process, such as Fe_2C , Fe_5C_2 and Fe_3C , etc. [9–14]. Hence, the research of the formation mechanism of iron carbides is significant to design the high-performance catalysts for FTS process.

The formation of carbon atoms via carburization gases dissociation on iron-based catalyst surfaces is the precondition for generation the iron carbides. The carbon atoms decomposed from carburization gases would diffuse into the iron lattice when the carbon chemical potentials of carburization gases are greater than that of iron carbides phase. The most studied carburization gases are CO and syngas,

because they have practical applications. Density Function Theory (DFT) calculations indicated that the presence of H₂ could accelerate the CO dissociation on metallic Fe (111) surfaces, suggesting that the syngas (H₂/CO) is an excellent carburization agent [15,16]. De Smit et al., using the in-situ setup (XAFS/XRD/Raman) under high pressure, investigated the carburization of α -Fe₂O₃ under different carbon chemical potentials (μ_c) in a syngas atmosphere and they found higher μ_c is beneficial to the formation of carbon-rich iron carbides [6]. Researchers also studied other carburization gases, such as C₂H₄ and C₂H₂ gas. These carbonaceous gases also could be partially dissociated into surface carbon and H₂ under FTS conditions, the surface carbon is a carbon source for the carburization of the iron-based catalysts [17–20]. Although these researchers made great efforts to investigate the influence of carburization gases, the intrinsic mechanism of carburization are still ambiguous, e.g., how the carburization gases were decomposed to form the surface carbon atoms, and then how the surface carbon atoms were permeated into the iron crystal lattice—all these issues need to be illuminated. In view of the carburization of the iron catalyst, the first step is the carbon atoms' formation which has not been fully researched on the micro level, so it is considered that the dissociation of the carburization gases into atomic carbon is necessary to be calculated in detail.

The important influence factor of the formation of carbon atoms via the dissociation of carburization gases is the catalyst promoter. The alkali metal and alkaline earth metal are the commonly studied promoters [21–24]. Thus far, the potassium promoter has been extensively applied in iron-based FTS catalysts, especially in commercial plants. It is well known that potassium promoter not only can increase the FTS activity, but also can increase the selectivity of higher molecular hydrocarbons and olefins [25–31]. It can be clearly found that all these researches mainly focused on the effect of potassium promoter to the catalytic performance of FTS [32–35], including the effect of the K₂O promoter on the morphology control to pure iron (α -Fe) [32] and Hägg carbide (Fe₅C₂) [34], as well as the hydrogenation mechanism of surface carbon [33] and CO [35] on the Fe₅C₂ surface; while the effect of promoter to the formation of carbon atoms from carburization gases on iron-based catalyst surface is hardly studied. In other words, the effect of the K₂O promoter on the decomposition ability of the carburization gases into the surface carbon atoms needs to be studied systematically on the iron catalysts' surfaces.

Using in situ XRD, Xu et al. recently studied the effect of varying carburization gases and potassium promoter on the carburization behaviors of α -Fe catalysts [36]. They reported that potassium could increase the carburization rate and in favor of the formation of carbon-rich iron carbides under CO or syngas, while the potassium promoter decreased the carburization rate and inhibited the formation of carbon-rich iron carbides under C₂H₄ or C₂H₂ atmosphere. Furthermore, via calculating the charge density difference, Bader charge and the adsorption energy of C₂H₄ and C₂H₂ on Fe(211) and Fe(211)-K₂O surface, they concluded that the potassium promoter could weaken the adsorption ability of C₂H₄ and C₂H₂ thermodynamically, which finally reduced the carburization capabilities of C₂H₄ and C₂H₂.

It has been reported that the percentage of the Fe(110) facet is predominant for un-promoted α -Fe catalysts, while the Fe(211) facet is dominated for potassium promoted α -Fe catalysts [32]. Therefore, the comparison of the carburization gases adsorption energies on Fe(100), Fe(110)-K₂O, Fe(211) and Fe(211)-K₂O surfaces would make sense for understanding the effect of K₂O promoter and designing the high-performance catalysts of FTS. In addition, the formation of atomic carbon via dissociation of carburization gases on these four facets also should be calculated, which is the precondition of carburization.

In this work, we used the GGA-PBE method to explore the adsorption energies and dissociation mechanisms of carburization gases on Fe(110), Fe(110)-K₂O, Fe(211) and Fe(211)-K₂O surfaces, respectively. Furthermore, on the basis of the calculation results, we identified the most favorable dissociation routes of carburization gases to form atomic carbon and gained the related rate constants. Our calculation results provide deep insights into the tuning effects of potassium promoter for the formation of carbon atoms via the dissociation process of CO/H₂, C₂H₄ and C₂H₂ gases on metallic

iron catalyst surfaces which well explained the experimental phenomen [36], and broaden the fundamental understanding of carburization behaviors of iron-based catalysts in the FTS process.

2. Results and Discussion

2.1. Adsorptions of C_2H_4 , C_2H_2 and CO/H_2 —The Initial Step of Carburization

As is well-known, carburization behavior of α -Fe catalyst is closely related on the nature of the catalyst and the pretreatment conditions. In the introduction, it has been mentioned that the Fe(110) surface is predominant for pure α -Fe catalysts and the Fe(211) facet is dominated for potassium-promoted α -Fe catalysts. Therefore, to understand the carburization behavior of the α -Fe catalyst at the atomic scale, we selected the Fe(110) and Fe(211) surfaces as the models of the α -Fe catalyst; firstly, we calculated the thermodynamic adsorption energies (E_{ads}) of carburization gases (C_2H_4 , C_2H_2 and CO/H_2) on the Fe(110), Fe(110)- K_2O , Fe(211) and Fe(211)- K_2O surfaces. The corresponding E_{ads} are listed in Table 1, and the top and side view configurations of C_2H_4 , C_2H_2 , CO and H_2 adsorption on the four surface models are given in Figure 1.

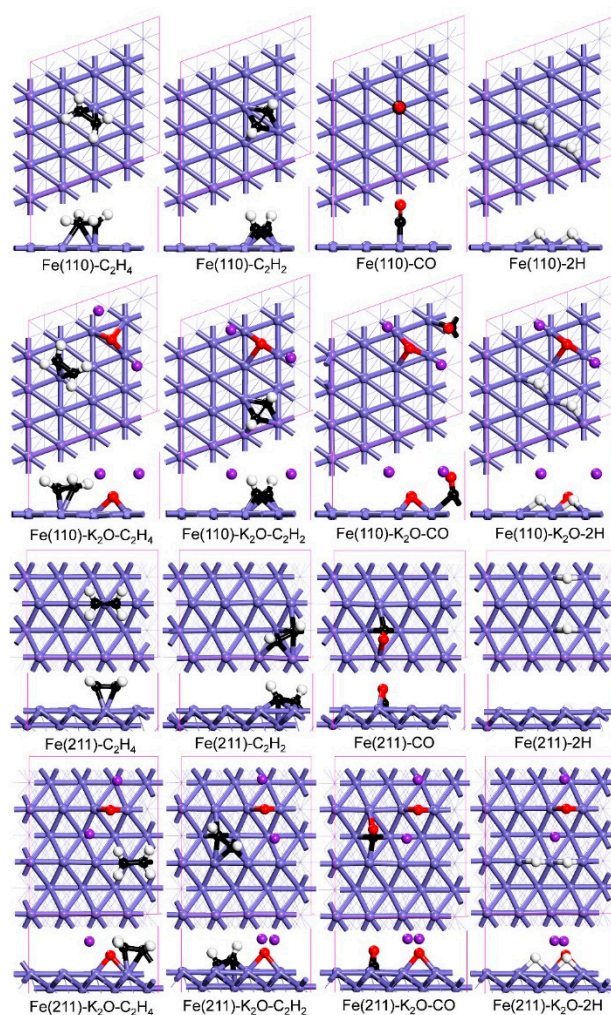


Figure 1. The top and side view configurations of C_2H_4 , C_2H_2 , CO and H_2 adsorption on the four surface models. The Fe, K, O, C and H atoms are given in grayish blue, purple, red, black and white, respectively.

Table 1. The adsorption energies (E_{ads} , eV) of the most stable C_2H_4 , C_2H_2 , CO and H_2 on the Fe(110), Fe(110)- K_2O , Fe(211) and Fe(211)- K_2O surfaces.

Surfaces	E_{ads} (eV)			
	CO	C_2H_4	C_2H_2	2H
Fe(110)	−2.00	−1.20	−3.39	−1.52
Fe(110)- K_2O	−2.28	−0.81	−3.03	−1.45
Fe(211)	−1.98	−1.36	−2.58	−1.14
Fe(211)- K_2O	−2.20	−1.23	−2.75	−1.46

In Table 1, it can be clearly seen that the CO adsorption energies on Fe(110)- K_2O and Fe(211)- K_2O are more negative than that on Fe(110) (−2.28 vs. −2.00 eV) and Fe(211) (−2.20 vs. −1.98 eV), suggesting the K_2O promoter could stabilize the adsorption of CO. However, the adsorption energies of the C_2H_4 molecule on Fe(110)- K_2O and Fe(211)- K_2O are more positive than that on Fe(110) (−0.81 vs. −1.20 eV) and Fe(211) (−1.23 vs. −1.36 eV), indicating the K_2O promoter could dramatically destabilize the adsorption of C_2H_4 . For the adsorption of C_2H_2 and H_2 , there is the opposite effect of the K_2O promoter on the two surfaces of Fe(110) and Fe(211). On the Fe(110)- K_2O facet, the C_2H_2 adsorption is much weaker than that on the clean Fe(110) facet (−3.03 vs. −3.39 eV), while it is stronger on the Fe(211)- K_2O facet than that on the clean Fe(211) facet (−2.75 vs. −2.58 eV). The effect of the K_2O promoter on H_2 adsorption energies on the selected facets are the same with that of C_2H_2 adsorption energies.

Totally, on the two surfaces of α -Fe catalysts, the CO and C_2H_4 adsorption can be stabilized and destabilized by the K_2O promoter, respectively, which is probably to explain the Xu's et al. experimental results thermodynamically—the K_2O promoter can enhance and inhibit the carburization capabilities of CO and C_2H_4 on α -Fe catalysts [36]. Nevertheless, the C_2H_2 acts as a probable intermediate species of C_2H_4 dissociation, its adsorption energies on the two surfaces are changed oppositely by the K_2O promoter. Therefore, it is inferred that, although the thermodynamic effect of K_2O promoter can partially explain the experimental phenomena, the dynamic influence is probably more important for the carburization behavior of α -Fe catalyst, which needs to be performed in detail.

In order to obtain a deep insight into the effect of the K_2O promoter on the four surface models of Fe(110), Fe(110)- K_2O , Fe(211) and Fe(211)- K_2O , the total Bader charge differences of Fe atoms (Δq) covered with and without surface species of C_2H_4 , C_2H_2 , CO and H_2 are analyzed in depth, and the detailed calculation method has been described in the Section 3.1. Meanwhile, the total Bader charge differences of Fe atoms in Fe(110) and Fe(211) covered with and without K_2O are also calculated (see Table 2).

Table 2. The total Bader charge differences (Δq) of Fe atoms on the four surface models covered with and without surface species (C_2H_4 , C_2H_2 , CO, H_2 and K_2O).

Surfaces	Δq				
	C_2H_4	C_2H_2	CO	2H	K_2O
Fe(110)	−0.49	−0.88	−0.41	−0.71	0
Fe(110)- K_2O	−0.65	−1.07	−0.77	−0.78	0.45
Fe(211)	−0.48	−1.07	−0.97	−0.68	0
Fe(211)- K_2O	−0.55	−1.20	−1.02	−0.80	0.46

For the adsorptions of C_2H_4 , C_2H_2 , CO and H_2 , all the Δq are negative on the four models, suggesting the electrons mainly transfer from Fe atoms to these surface species. In addition, it can be seen that the four Δq of Fe atoms on Fe(110)- K_2O and Fe(211)- K_2O (adsorbed with C_2H_4 , C_2H_2 , CO and H_2) are more negative than that of Fe(110) and Fe(211), suggesting the K_2O can promote the electron transfer from the surfaces to the adsorbed species. Then, the positive value of Δq (0.45 and 0.46) for K_2O adsorption on Fe(110) and Fe(211) further indicate that the electrons will be transferred

from K_2O to Fe atoms, which has been proved indirectly by the experimental results that the catalyst surface basicity could be modified by potassium promoter [37,38]. Therefore, it can be concluded that the electrons of the K_2O promoter will be transferred to the surface species via the Fe atoms in the catalyst surface. Furthermore, the same electronic transferring situation also can be seen from the charge density difference analysis of the surface adsorbed C_2H_4 , C_2H_2 , CO, H_2 and K_2O on the four models (see Figure 2).

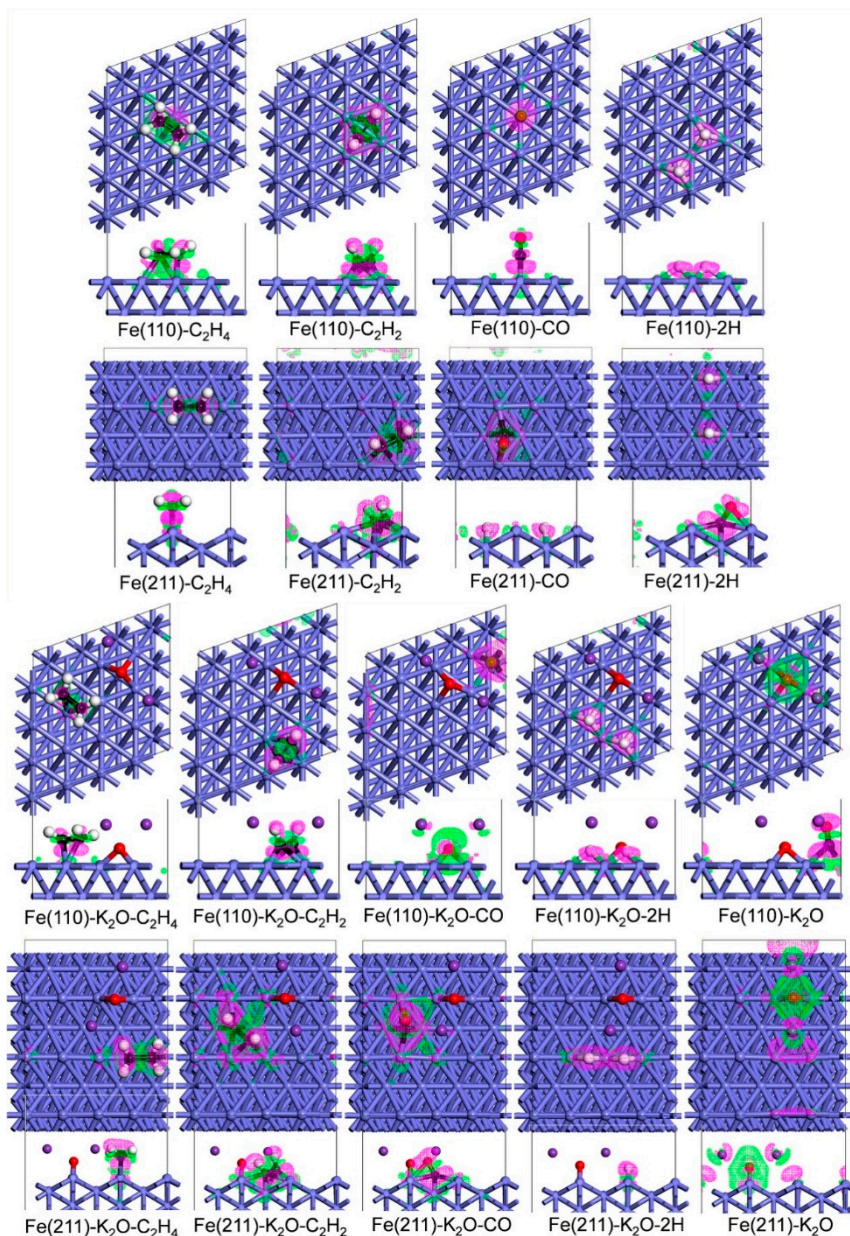


Figure 2. The charge density differences of surface adsorbed C_2H_4 , C_2H_2 , CO, H_2 and K_2O on the two models of Fe(110), Fe(211), Fe(110)- K_2O and Fe(211)- K_2O , the Fe, K, O, C and H atoms are given in grayish blue, purple, red, black and white, respectively; pink and green areas represent charge density accumulation and depletion, respectively; the cutoff of iso-surfaces is $0.005 \text{ electrons } \text{\AA}^{-3}$.

Via the above discussion, it is known that the K_2O promoter can stabilize the adsorption of CO, but destabilize the adsorption of C_2H_4 . However, in this part of work, the K_2O promoter has the same electronic properties for the different adsorption species. In a word, although the K_2O promoter as an electronic donor can afford electrons to all the different adsorbates, it has an obvious different effect

for different adsorption species. Based on a previous study [39], the chemical interactions are very complicated between the transition metal (TM) and the compounds of carbonyl (CO), carbene (C=C) and carbyne (C≡C). It was reviewed that the bonding model of TM-CO is obviously different from that of TM-C=C and TM-C≡C, e.g., the donor–acceptor interactions are considered as the dominant model of the TM-CO bond, while there is no electronic-back-donation in the bond of TM-C=C and TM-C≡C. Therefore, it is inferred that the different electronic interactions lead to the different effects of K₂O promoter on the CO, C₂H₄, C₂H₂ and H₂ adsorption.

2.2. Surface Atomic Carbon Formation—The Second Step of Carburization

In order to reveal essential role of the K₂O promoter during the carburization process, the formation routes of the surface C atoms via carburization gases dissociation are necessary to be investigated. In Figure 3, the most favorable pathways for C₂H₄/C₂H₂ dissociation into surface C atom on the Fe(110), Fe(110)-K₂O, Fe(211) and Fe(211)-K₂O, as well as the configurations of the corresponding intermediates, are shown. In Figure 3, the optimum routes of CO/H₂ dissociation into surface C atom on the four surfaces, as well as the corresponding structures of the intermediates are displayed. Meanwhile, for better comparing and understanding, all the barriers of the corresponding element steps, as well as the total effective barriers for C₂H₄/C₂H₂ and CO/H₂ dissociation on the four surfaces are also listed in Table 3. Furthermore, all the possible mechanisms of C₂H₄/C₂H₂ and CO/H₂ dissociation on the four surface models also have been given in the Supporting Information (Figures S1–S8).

2.2.1. Surface Atomic Carbon Formation via the Dissociations of C₂H₄/C₂H₂

On Fe(110) and Fe(110)-K₂O (see Figure 3 and Table 3), the most favorable steps of C₂H₄ dissociation begin with C₂H₄ dehydrogenation into the surface species of CHCH and two atomic H (C₂H₄ → CH₂CH + H → CHCH + 2H), the calculation barriers of CH₂CH formation are 0.37 and 0.39 eV on Fe(110) and Fe(110)-K₂O, and the CHCH formation barriers are 0.16 and 0.19 eV, respectively. Furthermore, their total reaction energies of C₂H₄ → CHCH + 2H on Fe(110) and Fe(110)-K₂O are −1.12 and −0.95 eV, suggesting the reaction can easily occur on two surfaces no matter from the view of thermodynamics or kinetics. After that, via the different paths, the C₂H₂ will be further dissociated into the surface 2C and 2H atoms (C₂H₂ → 2C + 2H) on the two surfaces.

For Fe(110), the C₂H₂ can directly dissociate into two CH species with a barrier of 0.81 eV, and the consequent decomposition of the two CH will form two surface C atoms with barriers of 0.72 and 1.17 eV. Here, we can clearly find that the second barrier of CH dissociation, as well as the adsorption properties of C+CH+3H to 2C+4H are significantly changed. Therefore, to explain about the differences, the Fe-Fe bond lengths and angles of the Fe(110) surface structures adsorbed with 2CH+2H, C+CH+3H and 2C+4H are compared in detail (see Figure S9). With the coverage increasing of the surface carbon atom, the structure of Fe(110) becomes distorted gradually, so it is considered that the changes of the second CH adsorption and reaction properties should be mainly attribute to the surface distortion. For Fe(110)-K₂O, the most favorable path for C₂H₂ dissociation forming surface C atoms is C₂H₂ → CCH + H → C + CH + H → 2C + 2H, and the three barriers are 0.99, 0.53 and 1.08 eV, respectively.

As a contrast, on Fe(211) and Fe(211)-K₂O, the favorable pathways (Figure 3) and the corresponding barriers (Table 3) of C₂H₄/C₂H₂ dissociation are investigated systematically. For the clean surface of Fe(211), the calculation results shown that the C₂H₄ will be firstly transferred into the ravine site from the ridge site with a barrier of 0.92 eV, and it is endothermic by 0.31 eV. With that, through the pathway of C₂H₄ → CH₂CH + H → CCH₂ + 2H → CCH + 3H → C₂ + 4H, the C₂H₄ in the ravine site can be further dissociated into a surface C₂ and four H atoms with four lower barriers of 0.49, 0.17, 0.68 and 0.82 eV. However, the subsequent decomposition of the surface C₂ is very difficult, which need a very high barrier of 1.95 eV, indicating the C-C bond cracking of the surface C₂ species (C₂ → 2C) is the rate-determining step. On Fe(211)-K₂O, although the ridge site of C₂H₄ can be directly dehydrogenated into the ridge site of CH₂CH and H atom (C₂H₄ → CH₂CH + H) with a barrier of 0.65 eV, the ridge site

of CH_2CH also needs to be transferred into the ravine site with a barrier of 0.69 eV. After that, with the route of $\text{CH}_2\text{CH} + \text{H} \rightarrow \text{CHCH} + 2\text{H} \rightarrow \text{CCH} + 3\text{H} \rightarrow \text{C}_2 + 4\text{H}$, the C_2H_3 in the ravine site can be further dehydrogenated into a surface C_2 and four H atoms with three lower barriers of 0.25, 0.35 and 0.30 eV. Nevertheless, the C-C bond cracking of the C_2 species ($\text{C}_2 \rightarrow 2\text{C}$) is also difficult because of the very high barrier of 1.75 eV. The formation of atomic carbons via C_2H_2 dissociation on Fe(211) facets are displayed in Figure S3, and the rated determining step is the C-C bond cracking of the C_2 species ($\text{C}_2 \rightarrow 2\text{C}$) which is the same with that of C_2H_4 dissociation.

For comparison, the K_2O promoter decreased the total effective barriers of the $\text{C}_2\text{H}_4/\text{C}_2\text{H}_2$ dissociation from 1.17 eV to 1.08 eV on the Fe(110) facet and from 2.04 eV to 1.75 eV on the Fe(211) facet, respectively. It can be concluded that the K_2O promoter can slightly improve the ability of forming atomic carbon via $\text{C}_2\text{H}_4/\text{C}_2\text{H}_2$ dissociation on Fe(110) and Fe(211) surface kinetically. However, this conclusion is contradictory with Xu et al.'s experimental results that the K_2O promoter can inhibit the carburization capabilities of C_2H_4 and C_2H_2 on α -Fe catalysts [36]. On the basis of the literature [32], it is known that the K_2O promoter can modify the exposed surface proportion of α -Fe catalysts. As increasing of K/Fe ratio, the percentage of Fe(211) is increased continuously from 32% to 70%, while the Fe(110) percentage is decreased from 39% to 20%. Surprisingly, it can be clearly found that the ability of atomic carbon formation from $\text{C}_2\text{H}_4/\text{C}_2\text{H}_2$ dissociation on Fe(211) and Fe(211)- K_2O are much harder than that on Fe(110) and Fe(110)- K_2O kinetically (2.04/1.75 vs. 1.17/1.08 eV). Therefore, it is reasonably inferred that the Fe(211) surface, tuned by the K_2O promoter, is attributed to the inhibiting of the carburization capabilities of C_2H_4 and C_2H_2 on α -Fe catalysts. In other words, the tuning effect of the K_2O promoter increases the exposed proportion of Fe(211), while it is exactly unfavorable the $\text{C}_2\text{H}_4/\text{C}_2\text{H}_2$ dissociation, and inhibits the carburization capabilities of C_2H_4 and C_2H_2 , which could well explain Xu et al.'s experimental results [36].

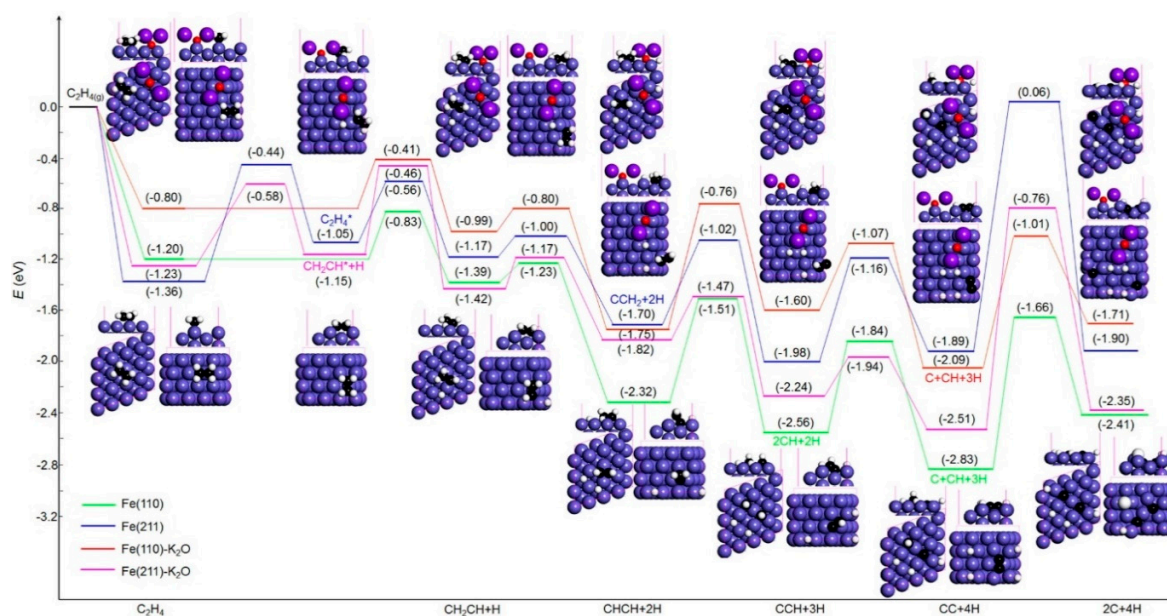


Figure 3. The most favorable pathways of $\text{C}_2\text{H}_4/\text{C}_2\text{H}_2$ dissociation on the Fe(110), Fe(110)- K_2O , Fe(211) and Fe(211)- K_2O , as well as the top and side view configurations of the corresponding intermediates. The Fe, K, O, C and H atoms are given in grayish blue, purple, red, black and white, respectively.

2.2.2. Surface Atomic Carbon Formation via the Dissociations of CO and CO/H_2

On Fe(110) and Fe(110)- K_2O surfaces (Figure 4 and Table 3), through three element steps of $\text{CO} + 2\text{H} \rightarrow \text{CHO} + \text{H} \rightarrow \text{CH} + \text{O} + \text{H} \rightarrow \text{C} + \text{O} + 2\text{H}$, the CO/H_2 will be dissociated into the surface C, O and H atoms. The calculation results shown that the three barriers are 1.31, 0.46 and 0.70 eV, respectively, on the Fe(110), suggesting the rate determining step is the first step of CHO formation

with a high barrier of 1.31 eV. Similarly, the three corresponding barriers are 1.65, 0.45 and 0.78 eV, and the formation of CHO also is the rate determining step on the Fe(110)-K₂O.

The mechanism of CO/H₂ dissociation on Fe(211) surfaces is significantly different from that on Fe(211)-K₂O surfaces. For the clean surface of Fe(211), the most favorable route is completely the same with that on the Fe(110) surface, the surface C formation from CO/H₂ decomposition needs three element steps of CO + 2H → CHO + H → CH + O + H → C + O + 2H, and the corresponding barriers are 0.72, 0.54 and 0.67 eV, respectively. For the K₂O-promoted surface of Fe(211)-K₂O, the optimal route is the direct dissociation of CO (CO + 2H → C + O + 2H), and the barrier is 0.77 eV.

In summary, it can be concluded that K₂O promoter enhanced the total effective barrier from 1.31 eV to 1.89 eV on Fe(110) surface, while reduced the total effective barriers from 1.26 eV to 0.77 eV on Fe(211) surface. This calculation results indicate that K₂O promoter has adverse effect on the ability of forming atomic carbon via CO/H₂ dissociation on Fe(110) and Fe(211) surfaces kinetically, i.e., they can inhibit and promote the CO decomposing, respectively. Similar with the analysis of the effect of K₂O promoter on the C₂H₄/C₂H₂ dissociation, it is inferred that the K₂O promoter increases the exposed proportion of Fe(211), and it is just beneficial to the CO/H₂ dissociation (1.26/0.77 vs. 1.31/1.89 eV), which enhances the carburization capability of CO/H₂, thus well explains the Xu et al.'s experimental result that the K₂O promoter can enhance the carburization capabilities of CO/H₂ on α-Fe catalysts [36].

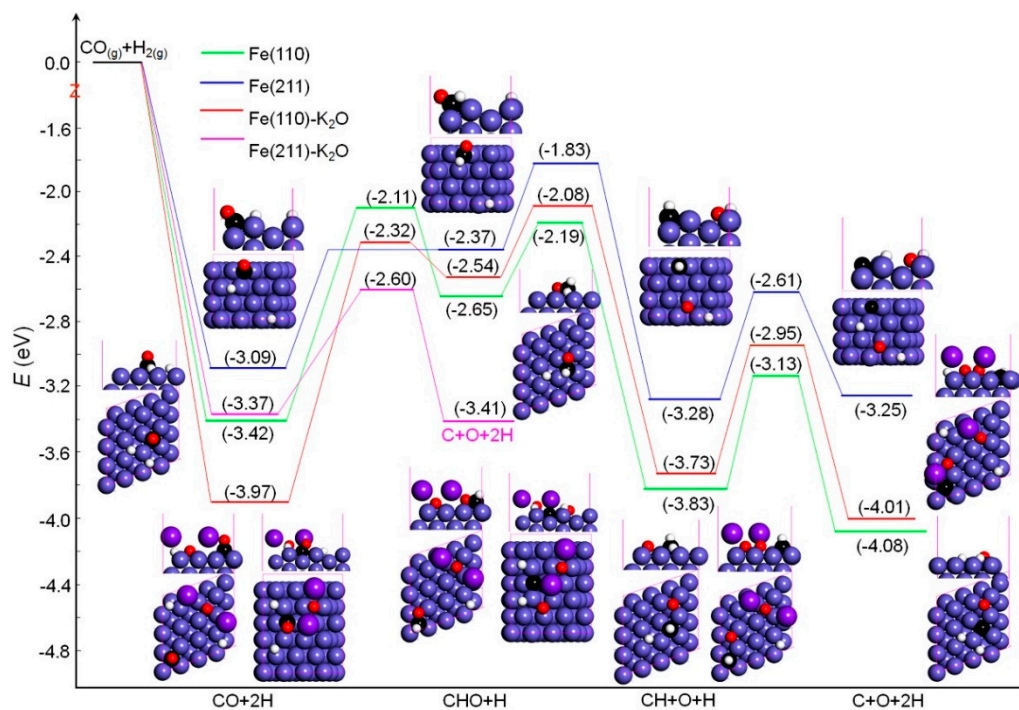


Figure 4. The most favorable pathways of CO/H₂ dissociation on the Fe(110), Fe(110)-K₂O, Fe(211) and Fe(211)-K₂O, as well as the top and side view of the configurations for the corresponding intermediates. The Fe, K, O, C and H atoms are given in grayish blue, purple, red, black and white, respectively.

2.3. Rate Constants of Elementary Steps

To get an in-depth understanding of the effect of potassium promoters on the formation process of surface atomic carbon on the metallic iron catalysts under different carburization gases, the rate constants (k , s⁻¹) of each element steps, as well as the total effective rate constants (k_{eff} , s⁻¹) of C₂H₄/C₂H₂ and CO/H₂ dissociation on Fe(110), Fe(110)-K₂O, Fe(211) and Fe(211)-K₂O were computed on the basis of the transition state theory [40,41]. The calculation method of the rate constant has been depicted in Section 3.1, and corresponding results are summarized in Table 3.

In Table 3, it can be clearly found that the rate-determining step of C_2H_4/C_2H_2 dissociation is the dehydrogenation of the second CH species ($C + CH + 3H \rightarrow 2C + 4H$) both on Fe(110) and Fe(110)- K_2O , while it is the C-C bond cracking ($CC + 4H \rightarrow 2C + 4H$) both on Fe(211) and Fe(211)- K_2O . As it is displayed, the rate constants of C_2H_4/C_2H_2 dissociation on Fe(110)- K_2O and Fe(211)- K_2O surfaces are about 10^2 times faster than that on Fe(110) and Fe(211) surfaces (Fe(110)- K_2O 3.30×10^3 vs. Fe(110) 6.79×10^1 , Fe(211)- K_2O 3.03×10^{-4} vs. Fe(211) 1.70×10^{-6}), so the K_2O promoter can enhance the C_2H_4/C_2H_2 dissociation rate on Fe(110) and Fe(211) surfaces.

For the decomposition of syngas (CO/ H_2), it can be known that the H-assisted dissociation of CO is the minimum energy paths, and the rate-determining step is the hydrogenation of CO into surface CHO ($CO + 2H \rightarrow CHO + H$) both on Fe(110), Fe(110)- K_2O and Fe(211). Nevertheless, the direct dissociation of CO is the favorable route ($CO + 2H \rightarrow C + O + 2H$) on Fe(211)- K_2O . Unlike the C_2H_4/C_2H_2 dissociation, the rate constants of CO/ H_2 dissociation on Fe(110)- K_2O facet is about 10^5 times slower than that on the Fe(110) facet (1.89×10^{-5} vs. 7.12×10^0) and it is about 10^4 times, on the Fe(211)- K_2O facet, faster than that on the Fe(211) facet (1.80×10^5 vs. 3.79×10^1), so the CO/ H_2 dissociation rate can be decreased by the K_2O promoter on Fe(110), while it can be increased on Fe(211).

However, it is also demonstrated that the C_2H_4/C_2H_2 dissociation rate constants on Fe(211) and Fe(211)- K_2O are about 10^7 times slower than that on Fe(110) and Fe(110)- K_2O (Fe(211) 1.70×10^{-6} vs. Fe(110) 6.79×10^1 , Fe(211)- K_2O 3.03×10^{-4} vs. Fe(110)- K_2O 3.30×10^3), while the dissociation rate constants of CO/ H_2 on Fe(211) are about five times faster than that on Fe(110) (3.79×10^1 vs. 7.12×10^0), and about 10^{10} times faster on Fe(211)- K_2O than on Fe(110)- K_2O (1.80×10^5 vs. 2.52×10^{-5}). Hence, the calculations of the rate constants further proved the above conclusions in Section 2.2 that the Fe(211) facet, tuned by the K_2O promoter, suppress the ability of C_2H_4/C_2H_2 carburization, but enhances the ability of CO/ H_2 carburization, which is well in agreement with the Xu's et al. experimental results.

Table 3. The barriers (E_a , eV) of the element steps for C_2H_4 and CO/H_2 dissociation, the rate constants (k , s^{-1}) at the temperature of 600K, as well as the total effective barriers (red boldface) and rate constants (blue boldface) of C_2H_4/C_2H_2 and CO/H_2 dissociation on Fe(110), Fe(110)- K_2O , Fe(211) and Fe(211)- K_2O surfaces.

Gases	Fe(110)					Fe(110)- K_2O				
	Element Steps	E_a	k	E_{eff}	k_{eff}	Element Steps	E_a	k	E_{eff}	k_{eff}
C_2H_4 or C_2H_2	$C_2H_4 \rightarrow C_2H_3 + H$	0.37	3.35×10^9	1.17	6.79×10^1	$C_2H_4 \rightarrow C_2H_3 + H$	0.39	1.22×10^9	1.08	3.30×10^3
	$C_2H_3 + H \rightarrow CHCH + 2H$	0.16	4.32×10^{11}			$C_2H_3 + H \rightarrow CHCH + 2H$	0.19	6.48×10^{11}		
	$CHCH + 2H \rightarrow 2CH + 2H$	0.81	2.42×10^5			$CHCH + 2H \rightarrow CCH + 3H$	0.99	9.54×10^3		
	$2CH + 2H \rightarrow C + CH + 3H$	0.72	2.41×10^5			$CCH + 2H \rightarrow C + CH + 3H$	0.53	3.73×10^7		
	$C + CH + 3H \rightarrow 2C + 4H$	1.17	6.79×10^1			$C + CH + 3H \rightarrow 2C + 4H$	1.08	3.30×10^3		
CO/H_2	$CO + 2H \rightarrow CHO + H$	1.31	7.12×10^0	1.31	7.12×10^0	$CO + 2H \rightarrow CHO + H$	1.65	1.51×10^{-2}	1.89	2.52×10^{-5}
	$CHO + H \rightarrow CH + O + H$	0.46	3.69×10^8			$CHO + H \rightarrow CH + O + H$	0.45	5.08×10^8		
	$CH + O + H \rightarrow C + O + 2H$	0.70	2.24×10^6			$CH + O + H \rightarrow C + O + 2H$	0.78	1.00×10^6		
gases	Fe(211)					Fe(211)- K_2O				
C_2H_4 or C_2H_2	C_2H_4 transition	0.92	4.33×10^3	2.04	1.70×10^{-6}	$C_2H_4 \rightarrow C_2H_3 + H$	0.65	2.00×10^7	1.75	3.03×10^{-4}
	$C_2H_4 \rightarrow C_2H_3 + H$	0.49	2.49×10^8			C_2H_3 transition	0.69	1.90×10^6		
	$C_2H_3 + H \rightarrow CCH_2 + 2H$	0.17	2.62×10^{11}			$C_2H_3 + H \rightarrow CHCH + 2H$	0.25	4.53×10^{10}		
	$CCH_2 + 2H \rightarrow CCH + 3H$	0.68	3.83×10^6			$CHCH + 2H \rightarrow CCH + 3H$	0.35	4.23×10^9		
	$CCH + 3H \rightarrow CC + 4H$	0.82	4.57×10^5			$CCH + 3H \rightarrow CC + 4H$	0.30	2.16×10^{10}		
	$CC + 4H \rightarrow 2C + 4H$	1.95	4.11×10^{-6}			$CC + 4H \rightarrow 2C + 4H$	1.75	3.03×10^{-4}		
CO/H_2	$CO + 2H \rightarrow CHO + H$	0.72	1.05×10^7	1.26	3.79×10^1	$CO + 2H \rightarrow C + O + 2H$	0.77	1.80×10^5	0.77	1.80×10^5
	$CHO + H \rightarrow CH + O + H$	0.54	4.09×10^7							
	$CH + O + H \rightarrow C + O + 2H$	0.67	5.27×10^6							

3. Methods and Models

3.1. Methods

In the Vienna Ab Initio Simulation Package (VASP) [42,43], the periodic plane wave-based method was used for all DFT calculations, in which the corresponding plane wave basis was set up to 400 eV, and the spin polarization was included. Specifically, the projector augmented wave (PAW) method was used to describe the electron–ion interaction [44,45], the generalized gradient approximation was adopted to deal with the electron exchange and correlation energies in the Perdew Burke Ernzerhof functional (GGA-PBE) [46]. Via the Methfessel-Paxton technique, the electron smearing width was set as 0.2 eV. Furthermore, the climbing image nudged elastic band method (CI-NEB) [47] was chosen to estimate the transition states, and their stretching frequencies were analyzed to evaluate whether the structure is a minimum or transition state without or with only one imaginary frequency.

According to $E_{\text{ads}} = E_{\text{A/surf}} - [E_{\text{surf}} + E_{\text{A}}]$, the adsorption energy of the adsorbates was calculated, where $E_{\text{A/surf}}$, E_{surf} and E_{A} is the total energy of the surface with adsorbates, the bare surface, and the free adsorbates in the gas phase. In a word, the more negative of E_{ads} represents the stronger adsorption. According to $\Delta E_{\text{r}} = E_{\text{FS}} - E_{\text{IS}}$ and $E_{\text{a}} = E_{\text{TS}} - E_{\text{IS}}$, the reaction energy (ΔE_{r}) and activation energy (E_{a}) are calculated, where E_{IS} , E_{TS} and E_{FS} are the corresponding energies of the initial state (IS), transition state (TS) and final state (FS), respectively.

Based on the transition state theory [40,41] the rate constants (k) of $\text{C}_2\text{H}_4/\text{C}_2\text{H}_2$ and CO/H_2 dissociation have been computed to distinguish the formation ability of surface atomic carbon from different carburization gases of $\text{C}_2\text{H}_4/\text{C}_2\text{H}_2$ and CO/H_2 on the Fe surfaces covered with and without the potassium promoter (the optimized models are given in Figure 5). The rate constant for element steps of the dissociation was calculated using Equation (1), in which k_{B} and h is the Boltzmann and Planck constant, T is the reaction temperature of 600 K, $q_{\text{TS,vib}}$ and $q_{\text{IS,vib}}$ are the harmonic vibrational partition functions of the transition and initial state, and E_{a} is the activation energy derived from DFT calculations. For $q_{\text{TS,vib}}$ and $q_{\text{IS,vib}}$, they were obtained according to Equation (2), in which the ν_i is the corresponding vibrational frequency for each vibrational mode of the surface intermediate.

$$k = \frac{k_{\text{B}}T}{h} \frac{q_{\text{TS,vib}}}{q_{\text{IS,vib}}} e^{-E_{\text{a}}/k_{\text{B}}T} \quad (1)$$

$$q_{\text{vib}} = \prod_i \frac{1}{1 - \exp(-\frac{h\nu_i}{k_{\text{B}}T})} \quad (2)$$

The total Bader charge difference of Fe atoms (Δq) covered with and without surface species was calculated according to Equation (3) as follows.

$$\Delta q = q_{\text{A/surf}} - q_{\text{surf}} \quad (3)$$

where $q_{\text{A/surf}}$ is the total Bader charge of all the Fe atoms in the Fe(110), Fe(110)-K₂O, Fe(211) and Fe(211)-K₂O covered with surface species of C_2H_4 , C_2H_2 , CO and H_2 , while the q_{surf} is the total Bader charge of all the Fe atoms in the corresponding clean surface.

3.2. Models

The lattice constant of cubic Fe cell (bcc) is calculated; Its value is well in agreement with that of the experiment (2.831 vs. 2.866 Å), and the Fe-Fe bond length is 2.452 Å. In Figure 5, the top and side view structures of Fe(110), Fe(110)-K₂O, Fe(211) and Fe(211)-K₂O are shown, and the unit cells p(4×4), p(4×4), p(4×2) and p(4×3) were chosen for these four surfaces, respectively. For both the four surface models, the 3×3×1 k-point sampling was used. Totally, there are four atomic layers in the Fe(110) and Fe(110)-K₂O, including 64 Fe atoms, of which 16 were fixed. In Fe(211) and Fe(211)-K₂O, eight atomic

layers are used, the former includes 64 Fe atoms, of which 24 were fixed, while the latter includes 96 Fe atoms, of which 36 were fixed.

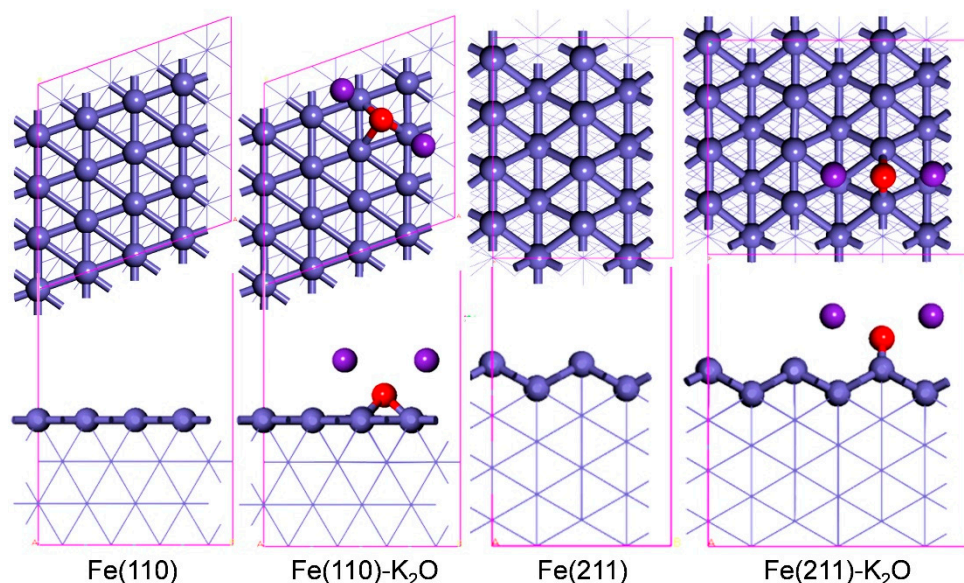


Figure 5. The top and side view of the surface models for the Fe(110), Fe(110)-K₂O, Fe(211) and Fe(211)-K₂O. The Fe, K and O atoms are given in grayish blue, purple and red, respectively.

4. Conclusions

In this work, in order to illuminate the essential effect of the potassium promoter on the generation of atomic carbon via carburization gases dissociation on the iron-based catalyst, the C₂H₄, C₂H₂ and CO/H₂ adsorptions and decompositions, as well as the rate constants of the corresponding elementary steps, are investigated by Density Function Theory on the Fe(110), Fe(110)-K₂O, Fe(211) and Fe(211)-K₂O surfaces. The calculation results suggest that the K₂O promoter can modify the capabilities of surface C formation under different carburization gases via the thermodynamic method as well as the kinetical method, which also can explain the experiment results well [36].

Thermodynamically, the K₂O promoter can increase the CO adsorption energy while decreasing the adsorption energy of the C₂H₄ molecule on both the Fe(110) and Fe(211) surfaces, which can explain the experiment results that the K₂O promoter can enhance and inhibit the carburization capabilities of CO and C₂H₄ on α -Fe catalysts. Nevertheless, the adsorption energies of C₂H₂ and H₂ were decreased on the Fe(110), while their adsorption energies were increased on Fe(211) by the K₂O promoter. Therefore, it is inferred that the thermodynamic and kinetic effects of K₂O promoter can jointly controlled the carburization behavior of α -Fe catalysts.

Kinetically, comparing with Xu's et al. experimental results, although the calculations originally obtain a contradictory conclusion that the K₂O promoter can slightly improve the ability of forming atomic C via C₂H₄/C₂H₂ dissociation on Fe(110) and Fe(211), while suppressing the atomic C formation via CO/H₂ decomposition on Fe(110). However, via the detailed analysis of the literature [32] and calculation results, it is finally inferred that the tuning effect of the K₂O promoter on the catalyst surfaces increases the exposed proportion of Fe(211), which exactly inhibits the C₂H₄/C₂H₂ dissociation, while enhancing the CO/H₂ decomposition, and the conclusion could well explain the experimental results of Xu et al. [36].

It is believed that different surfaces of iron carbides have different reactivity in the FTS process, i.e., high-performance catalysts could be designed via catalyst-preparing technology which could control exposing facets of the iron-based catalyst. Hence, there are some potential routes which could be suggested based on our calculations and the literature for designing high-performance catalysts in the FTS process: (a) controlling the proportion of exposed surfaces of iron-based catalysts by the

surface science and technology; (b) changing the composition and proportion of carburization gases; (c) modulating the order of carburization and K₂O promoter addition during the catalysts' preparation process; (d) adding some other metal oxide replacing the K₂O promoter, such as the reported Na₂O [24].

Supplementary Materials: The following are available online at <http://www.mdpi.com/2073-4344/10/5/527/s1>, Figure S1. The energy profiles of C₂H₄ dissociation on Fe(110), as well as the top and side view of the configurations for the corresponding intermediates. Figure S2. The energy profiles of C₂H₄ dissociation on Fe(110)-K₂O, as well as the top and side view of the configurations for the corresponding intermediates. Figure S3. The energy profiles of C₂H₄ dissociation on Fe(211), as well as the top and side view of the configurations for the corresponding intermediates. Figure S4. The energy profiles of C₂H₄ dissociation on Fe(211)-K₂O, as well as the top and side view of the configurations for the corresponding intermediates. Figure S5. The energy profiles of CO/H₂ dissociation on Fe(110), as well as the top and side view of the configurations for the corresponding intermediates. Figure S6. The energy profiles of CO/H₂ dissociation on Fe(110)-K₂O, as well as the top and side view of the configurations for the corresponding intermediates. Figure S7. The energy profiles of CO/H₂ dissociation on Fe(211), as well as the top and side view of the configurations for the corresponding intermediates. Figure S8. The energy profiles of CO/H₂ dissociation on Fe(211)-K₂O, as well as the top and side view of the configurations for the corresponding intermediates. Figure S9. The top and side view structures of 2CH+H, C+CH+3H and 2C+4H on Fe(110). Table S1. The distances between the two atoms (d , Å) to be dissociated in the transition states of the element steps for C₂H₄ and CO/H₂ dissociation on Fe(110), Fe(110)-K₂O, Fe(211) and Fe(211)-K₂O surfaces.

Author Contributions: Conceptualization, R.G.; Data curation, C.C. and H.H.; Formal analysis, C.C. and R.S.; Investigation, J.G.; Methodology, L.C.; Software, L.C.; Supervision, R.G. and H.H.; Visualization, C.C. and R.S.; Writing—original draft, J.G.; Writing—review & editing, R.G. and H.H. All authors have read and agreed to the published version of the manuscript.

Funding: This research was funded by the the National Natural Science Foundation of China (No.21802076, 21962013), Program of Higher-level Talents of IMU (No.21300-5185111, No.21300-5185109).

Acknowledgments: The authors are grateful for the financial support from the National Natural Science Foundation of China (No.21802076, 21962013), Program of Higher-level Talents of IMU (No.21300-5185111, No.21300-5185109). We also acknowledge Synfuels China, Co. Ltd. And National Supercomputing Center in Shenzhen (Shenzhen Cloud Computing Center) for their Super-Server for the DFT calculations.

Conflicts of Interest: The authors declare no conflict of interest.

References

1. Yu, J.; Ju, Y.; Zhao, L.; Chu, X.; Yang, Z.; Tian, Y.; Sheng, F.; Lin, J.; Liu, F.; Dong, Y.; et al. Multistimuli-Regulated Photochemical Cancer Therapy Remotely Controlled via Fe₅C₂ Nanoparticles. *ACS Nano* **2015**, *10*, 159–169. [CrossRef] [PubMed]
2. Giordano, C.; Kraupner, A.; Wimbush, S.C.; Antonietti, M. Iron Carbide: An Ancient Advanced Material. *Small* **2010**, *6*, 1859–1862. [CrossRef] [PubMed]
3. Zhao, Y.; Zhang, J.; Guo, X.; Fan, H.; Wu, W.; Liu, H.; Wang, G. Fe₃C@nitrogen doped CNT arrays aligned on nitrogen functionalized carbon nanofibers as highly efficient catalysts for the oxygen evolution reaction. *J. Mater. Chem. A* **2017**, *5*, 19672–19679. [CrossRef]
4. Wirth, C.T.; Bayer, B.C.; Gamalski, A.D.; Esconjauregui, S.; Weatherup, R.; Ducati, C.; Baehtz, C.; Robertson, J.; Hofmann, S. The Phase of Iron Catalyst Nanoparticles during Carbon Nanotube Growth. *Chem. Mater.* **2012**, *24*, 4633–4640. [CrossRef]
5. Chang, Q.; Zhang, C.H.; Liu, C.W.; Wei, Y.X.; Cheruvathur, A.V.; Dugulan, A.I.; Niemantsverdriet, J.W.; Liu, X.W.; He, Y.R.; Qing, M.; et al. Relationship between iron carbide phases (ϵ -Fe₂C, Fe₇C₃, and χ -Fe₅C₂) and catalytic performances of Fe/SiO₂ fischer-tropsch catalysts. *ACS Catal.* **2018**, *8*, 3304–3316. [CrossRef]
6. De Smit, E.; Cinquini, F.; Beale, A.M.; Safonova, O.V.; van Beek, W.; Sautet, P.; Weckhuysen, B.M. Stability and reactivity of epsilon-chi-theta iron carbide catalyst phases in Fischer-Tropsch synthesis: Controlling μ C. *J. Am. Chem. Soc.* **2010**, *132*, 14928–14941. [CrossRef]
7. Petersen, M.A.; Berg, J.-A.V.D.; Van Rensburg, W.J. Role of Step Sites and Surface Vacancies in the Adsorption and Activation of CO on χ -Fe₅C₂ Surfaces. *J. Phys. Chem. C* **2010**, *114*, 7863–7879. [CrossRef]
8. Xu, J.; Bartholomew, C.H. Temperature-Programmed Hydrogenation (TPH) and in Situ Mössbauer Spectroscopy Studies of Carbonaceous Species on Silica-Supported Iron Fischer-Tropsch Catalysts. *J. Phys. Chem. B* **2005**, *109*, 2392–2403. [CrossRef]
9. Amelse, J.A.; Butt, J.B.; Schwartz, L.H. Carburization of supported iron synthesis catalysts. *J. Phys. Chem.* **1978**, *82*, 558–563. [CrossRef]

10. Raupp, G.B.; Delgass, W.N. Delgass, Mossbauer investigation of supported Fe and FeNi catalysts: II. Carbides formed by Fischer-Tropsch synthesis. *J. Catal.* **1979**, *58*, 348–360. [[CrossRef](#)]
11. Niemantsverdriet, J.W.; Van Der Kraan, A.M.; Van Dijk, W.L.; Van Der Baan, H.S. Behavior of metallic iron catalysts during Fischer-Tropsch synthesis studied with Mössbauer spectroscopy, x-ray diffraction, carbon content determination, and reaction kinetic measurements. *J. Phys. Chem.* **1980**, *84*, 3363–3370. [[CrossRef](#)]
12. Lecaer, G.; Dubois, J.M.; Pijolat, M.; Perrichon, V.; Bussiere, P. Characterization by Mossbauer-spectroscopy of iron carbides formed by Fischer-Tropsch synthesis. *J. Phys. Chem.* **1982**, *86*, 4799–4808. [[CrossRef](#)]
13. Mansker, L.D.; Jin, Y.; Bukur, D.B.; Datye, A. Characterization of slurry phase iron catalysts for Fischer-Tropsch synthesis. *Appl. Catal. A Gen.* **1999**, *186*, 277–296. [[CrossRef](#)]
14. Li, S.; Meitzner, G.D.; Iglesia, E. Structure and Site Evolution of Iron Oxide Catalyst Precursors during the Fischer-Tropsch Synthesis. *J. Phys. Chem. B* **2001**, *105*, 5743–5750. [[CrossRef](#)]
15. Arakawa, H.; Bell, A.T. Effects of potassium promotion on the activity and selectivity of iron Fischer-Tropsch catalysts. *Ind. Eng. Chem. Process. Des. Dev.* **1983**, *22*, 97–103. [[CrossRef](#)]
16. Huo, C.-F.; Ren, J.; Li, Y.-W.; Wang, J.; Jiao, H. CO dissociation on clean and hydrogen precovered Fe(111) surfaces. *J. Catal.* **2007**, *249*, 174–184. [[CrossRef](#)]
17. Erley, W.; Baro, A.M.; Ibach, H. Vibrational-spectra of acetylene and ethylene adsorbed on Fe(110). *Surf. Sci.* **1982**, *120*, 273–290. [[CrossRef](#)]
18. Seip, U.; Tsai, M.C.; Kuppers, J.; Ertl, G. Interaction of acetylene and ethylene with an Fe(111) surface. *Surf. Sci.* **1984**, *147*, 65–88. [[CrossRef](#)]
19. Hung, W.-H.; Bernasek, S. Adsorption and decomposition of ethylene and acetylene on Fe(100). *Surf. Sci.* **1995**, *339*, 272–290. [[CrossRef](#)]
20. Booyens, S.; Gilbert, L.; Willock, D.; Bowker, M. The adsorption of ethene on Fe(111) and surface carbide formation. *Catal. Today* **2015**, *244*, 122–129. [[CrossRef](#)]
21. Li, J.; Zhang, C.; Cheng, X.; Qing, M.; Xu, J.; Wu, B.; Yang, Y.; Li, Y. Effects of alkaline-earth metals on the structure, adsorption and catalytic behavior of iron-based Fischer-Tropsch synthesis catalysts. *Appl. Catal. A Gen.* **2013**, *464*, 10–19. [[CrossRef](#)]
22. Li, J.; Cheng, X.; Zhang, C.; Yang, Y.; Li, Y. Effects of alkali on iron-based catalysts for Fischer-Tropsch synthesis: CO chemisorptions study. *J. Mol. Catal. A Chem.* **2015**, *396*, 174–180. [[CrossRef](#)]
23. Li, J.; Cheng, X.; Zhang, C.; Chang, Q.; Wang, J.; Wang, X.; Lv, Z.; Dong, W.-S.; Yang, Y.; Li, Y. Effect of alkalis on iron-based Fischer-Tropsch synthesis catalysts: Alkali-FeO_x interaction, reduction, and catalytic performance. *Appl. Catal. A Gen.* **2016**, *528*, 131–141. [[CrossRef](#)]
24. Zhai, P.; Xu, C.; Gao, R.; Liu, X.; Li, M.; Li, W.; Fu, X.; Jia, C.; Xie, J.; Zhao, M.; et al. Highly Tunable Selectivity for Syngas-Derived Alkenes over Zinc and Sodium-Modulated Fe₅C₂ Catalyst. *Angew. Chem. Int. Ed.* **2016**, *55*, 9902–9907. [[CrossRef](#)]
25. Crowell, J.E.; Somorjai, G.A. The effect of potassium on the chemisorption of carbon monoxide on the Rh(111) crystal face. *Appl. Surf. Sci.* **1984**, *19*, 73–91. [[CrossRef](#)]
26. Raje, A.P.; O'Brien, R.J.; Davis, B.H. Effect of Potassium Promotion on Iron-Based Catalysts for Fischer-Tropsch Synthesis. *J. Catal.* **1998**, *180*, 36–43. [[CrossRef](#)]
27. Bukur, D.B.; Mukesh, D.; Patel, S.A. Promoter effects on precipitated iron catalysts for Fischer-Tropsch synthesis. *Ind. Eng. Chem. Res.* **1990**, *29*, 194–204. [[CrossRef](#)]
28. Herzog, K.; Gaube, J. Kinetic studies for elucidation of the promoter effect of alkali in Fischer-Tropsch iron catalysts. *J. Catal.* **1989**, *115*, 337–346. [[CrossRef](#)]
29. Gaube, J.; Klein, H.-F. The promoter effect of alkali in Fischer-Tropsch iron and cobalt catalysts. *Appl. Catal. A Gen.* **2008**, *350*, 126–132. [[CrossRef](#)]
30. Dry, M. The correlation between catalyst surface basicity and hydrocarbon selectivity in the Fischer-Tropsch synthesis. *J. Catal.* **1968**, *11*, 18–24. [[CrossRef](#)]
31. Dry, M. Heats of chemisorption on promoted iron surfaces and the role of alkali in Fischer-Tropsch synthesis. *J. Catal.* **1969**, *15*, 190–199. [[CrossRef](#)]
32. Huo, C.-F.; Wu, B.-S.; Li, Y.-W.; Gao, P.; Yang, Y.; Jiao, H. The Mechanism of Potassium Promoter: Enhancing the Stability of Active Surfaces. *Angew. Chem. Int. Ed.* **2011**, *50*, 7403–7406. [[CrossRef](#)] [[PubMed](#)]
33. Zhao, S.; Liu, X.-W.; Huo, C.-F.; Li, Y.-W.; Wang, J.; Jiao, H. The role of potassium promoter in surface carbon hydrogenation on Hägg carbide surfaces. *Appl. Catal. A Gen.* **2015**, *493*, 68–76. [[CrossRef](#)]

34. Zhao, S.; Liu, X.-W.; Huo, C.-F.; Wen, X.-D.; Guo, W.; Cao, D.; Yang, Y.; Li, Y.-W.; Wang, J.; Jiao, H. Morphology control of K₂O promoter on Hägg carbide (χ -Fe₅C₂) under Fischer–Tropsch synthesis condition. *Catal. Today* **2016**, *261*, 93–100. [[CrossRef](#)]
35. Zhao, S.; Liu, X.-W.; Huo, C.-F.; Li, Y.-W.; Wang, J.; Jiao, H. Potassium promotion on CO hydrogenation on the χ -Fe 5 C 2 (111) surface with carbon vacancy. *Appl. Catal. A Gen.* **2017**, *534*, 22–29. [[CrossRef](#)]
36. Niu, L.; Liu, X.; Liu, J.; Liu, X.; Wen, X.; Yang, Y.; Xu, J.; Li, Y. Tuning carburization behaviors of metallic iron catalysts with potassium promoter and CO/syngas/C₂H₄/C₂H₂ gases. *J. Catal.* **2019**, *371*, 333–345. [[CrossRef](#)]
37. Lohitharn, N.; Goodwin, J.G.; Goodwinjr, J. Effect of K promotion of Fe and FeMn Fischer–Tropsch synthesis catalysts: Analysis at the site level using SSITKA. *J. Catal.* **2008**, *260*, 7–16. [[CrossRef](#)]
38. Yang, Y.; Xiang, H.W.; Xu, Y.Y.; Bai, L.; Li, Y.W. Effect of potassium promoter on precipitated iron-manganese catalyst for Fischer–Tropsch synthesis. *Appl. Catal. A Gen.* **2004**, *266*, 181–194. [[CrossRef](#)]
39. Frenking, G.; Fröhlich, N. The nature of the bonding in transition-metal compounds. *Chem. Rev.* **2000**, *100*, 717–774. [[CrossRef](#)]
40. Eyring, H. The Activated Complex in Chemical Reactions. *J. Chem. Phys.* **1935**, *3*, 107. [[CrossRef](#)]
41. Lu, J.; Behtash, S.; Faheem, M.; Heyden, A. Microkinetic modeling of the decarboxylation and decarbonylation of propanoic acid over Pd(111) model surfaces based on parameters obtained from first principles. *J. Catal.* **2013**, *305*, 56–66. [[CrossRef](#)]
42. Kresse, G.; Furthmüller, J. Efficiency of ab-initio total energy calculations for metals and semiconductors using a plane-wave basis set. *Comput. Mater. Sci.* **1996**, *6*, 15–50. [[CrossRef](#)]
43. Kresse, G.; Furthmüller, J. Efficient iterative schemes for ab initio total-energy calculations using a plane-wave basis set. *Phys. Rev. B* **1996**, *54*, 11169–11186. [[CrossRef](#)] [[PubMed](#)]
44. Blochl, P.E. Projector augmented-wave method. *Phys. Rev. B* **1994**, *50*, 17953–17979. [[CrossRef](#)]
45. Kresse, G.; Joubert, D. From ultrasoft pseudopotentials to the projector augmented-wave method. *Phys. Rev. B* **1999**, *59*, 1758–1775. [[CrossRef](#)]
46. Perdew, J.P.; Burke, K.; Ernzerhof, M. Generalized Gradient Approximation Made Simple. *Phys. Rev. Lett.* **1996**, *77*, 3865–3868. [[CrossRef](#)]
47. Henkelman, G.; Uberuaga, B.P.; Jónsson, H. A climbing image nudged elastic band method for finding saddle points and minimum energy paths. *J. Chem. Phys.* **2000**, *113*, 9901–9904. [[CrossRef](#)]



© 2020 by the authors. Licensee MDPI, Basel, Switzerland. This article is an open access article distributed under the terms and conditions of the Creative Commons Attribution (CC BY) license (<http://creativecommons.org/licenses/by/4.0/>).